Pergamon

Acta mater. Vol. 46, No. 1, pp. 101–110, 1998

Printed in Great Britain
PII: S1359-6454(97)00222-X
1359-6454/98 $19.00 + 0.00

X-RAY DIFFRACTION CHARACTERIZATION OF HEAVILY DEFORMED METALLIC SPECIMENS

L. LUTTEROTTI* and S. GIALANELLA

Dipartimento di Ingegneria dei Materiali, Università di Trento, 38050, Mesiano, Italy

(Received 12 March 1997; accepted 15 July 1997)

Abstract—Ordered intermetallic compound powders can be heavily deformed and disordered by ball-milling. This highly energetic deformation process introduces several kinds of defects into the powder and changes the aspect of the grains. By a novel analysis of the diffraction spectra we can analyse most of such defects and characterize the correlation between the shape of the powder and its crystallographic orientation. In this way we can also recognize how deformation may occur along specific crystallographic planes. The quantitative evaluation of dislocations, twins, stacking and deformation faultings allows us to correlate the disordering process to the introduction and development of defects under the effect of milling. It is shown how a full pattern fitting of diffraction spectra can be successfully applied to a comprehensive investigation of a material modification process, if appropriate physical models are used to describe the scattering event instead of semiempirical functions. © *1997 Acta Metallurgica Inc.*

1. INTRODUCTION

The effects of deformations on the microstructure of metallic materials can be profitably investigated using transmission electron microscopy (TEM) and X-ray diffraction (XRD). TEM observations afford direct pictures of the deformed regions with the possibility of identifying, using suitable imaging conditions, such lattice defects as vacancies, dislocations, stacking faults, etc. However the attainment of reliable results is largely dependent on the care used in the preparation of thin sections to be observed. Indeed the resulting microstructure may no longer be representative of the original structure, owing to the defects introduced or removed during the thinning procedure. In the case of highly unstable or metastable structures, sample preparation may also induce phase transformations so that the actually observed structure might be quite different from the original one. Another factor limiting the capabilities of TEM investigations is the poor quality of the images attainable from specimens featuring extremely elevated concentrations of lattice defects, such as dislocations. For these reasons other techniques, such as XRD, are sometime interesting alternatives to TEM in the characterization of materials. Sample preparation for XRD analyses is generally very straightforward and no artifacts affect the experimental data, unless mistakes are made, for instance, when positioning the sample in the goniometer. A significant computational effort is needed in order to get from the raw diffraction patterns all possible information regarding the microstructure of the analysed specimens. For doing this, a number of methods have been developed over the years, fully described in the classical textbook on XRD techniques [1].

The remarkable calculus capabilities available nowadays in user friendly personal computers, often directly connected to X-ray diffraction apparatuses, have contributed to an ever increasing spreading of data analysis programs based on the so-called Rietveld method [2].

In the present study an already existing Rietveld routine [3] has been developed further by the addition of other parameters accounting for the effects on the simulated diffraction pattern of the crystallite size and r.m.s. (root mean squares) microstrain, texture, planar defects, antiphase domain size and different degrees of long-range order, as far as ordered intermetallics are concerned.

In order to test this new method the results obtained from the study of ball-milled Ni_3Al powders are presented. Some conclusions on the applicability and reliability of the method will be drawn at the end.

2. X-RAY DIFFRACTION METHODOLOGY

The original Rietveld method was developed to refine a crystal structure from powder diffraction, when single crystal data are not available. It consists of a calculus routine which can fit the whole powder diffraction spectrum [2, 4]. Subsequently the approach was applied also to quantitative phase analysis [5, 6]. It has recently been proposed as a procedure which includes the Rietveld refinement texture and residual stresses [7–11].

*To whom all correspondence should be addressed.

In the present work deformation faults, antiphase domain boundaries and the roughness are also accounted for, in modelling the spectra, using a more comprehensive approach. In the Rietveld refinement the background and peak profiles for all phases present in the sample are evaluated. Background is usually described by a polynomial function. For each reflection, the profile is defined by the angular position, the intensity and the peak shape. The position and the intensity are evaluated from the crystal structure and phase composition. The peak profile can be described as a Pseudo-Voigt, Voigt or Pearson VII function defined by a half-width at half-maximum (HWHM) and a shape parameter (the so-called Gaussian content in the Pseudo-Voigt case). The methodology can be easily extended to include residual stresses, texture and microstructure contributions, i.e. crystallite size, microstrain and defect concentrations. Indeed the stress field modifies the peak positions, the texture of the sample affects the integrated intensities of the reflections and the microstructure changes the shape of the profiles.

In the present approach the intensity of a diffraction peak is considered to be composed of a so-called random intensity, corresponding to that of an ideally randomly oriented sample, multiplied by a texture factor (the pole density) and a correction factor for the roughness of the sample. Therefore the intensity of an (*hkl*) reflection collected at α, β tilting angles (see Fig. 1 for the definition of these angles) is given by:

$$I_{hkl}(\alpha, \beta) = (1 - R) I_{hkl}^{\text{rand}} P_{hkl}(\alpha, \beta), \tag{1}$$

where R is the roughness correction, $I_{\text{hkl}}^{\text{rand}}$ is the intensity for the random orientation of the diffraction line with Miller indices h, k, l, and $P_{hkl}(\alpha, \beta)$ is the texture correction coefficient. $I_{\text{hkl}}^{\text{rand}}$ can be computed from the structure factor of the phase and contains some geometrical aberration terms.

The degree of the long-range order, in the case of ordered alloys, depends on the site occupancy, which affects the structure factor and can be therefore refined in the fitting procedure. In our case we have two different atoms and two kind of sites, that means four occupancy values to refine. Using the definitions in Appendix A and the relationships between composition and occupancy it is possible to reduce the number of unknown parameters to only one.

The long-range order parameter S, for a binary alloy (A_xB_y) having a crystal structure with two kinds of atomic positions (α and β sites), can be evaluated according to the relationships proposed by Warren [12] and recalled in Appendix A. The occupancy factors w_α, r_β and w_β, are given, in terms of the alloy composition and the parameter r_α (Appendix A), by the following expressions:

$$\begin{aligned} w_\beta &= \frac{x_{\text{A}} - r_\alpha y_\alpha}{y_\beta}, \\ w_\alpha &= 1 - r_\alpha, \\ r_\beta &= 1 - w_\beta = 1 - \frac{x_{\text{A}} - r_\alpha y_\alpha}{y_\beta}. \end{aligned} \tag{2}$$

The long-range order parameter is given by:

$$S = r_\alpha - \frac{x_{\text{A}} - r_\alpha y_\alpha}{y_\beta}. \tag{3}$$

The correction factor R in the equation (1) is evaluated from the model for roughness correction formulated by Hermann and Ermrich [13]:

$$R = P_0 + C \frac{\tau}{\sin\theta \cos\alpha} \left(1 - \frac{\tau}{\sin\theta \cos\alpha}\right), \tag{4}$$

where P_0, C and τ are parameters to be refined. With respect to the original formula, the term $\cos\alpha$ is introduced to take into account the possible tilting of the sample in our experimental configuration (Fig. 1).

For the pole density P_{hkl}, the harmonic approximation introduced by Bunge [14] and Roe [15], is used. According to [7], P_{hkl} (α, β) is proportional to the volume fraction of crystallites having the [*hkl*]

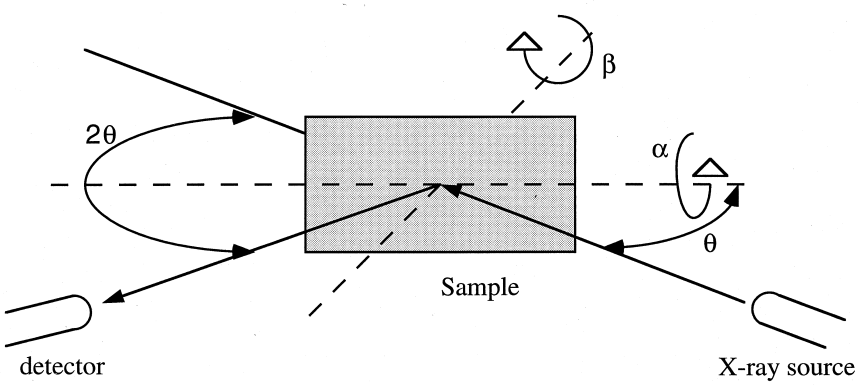

Fig. 1. Sketch of the diffraction geometry used for the texture measurement, α is the polar angle and β the azimuthal one.

direction parallel to the α, β orientation. This factor can be expanded into a series of harmonic functions described by a certain number of harmonic coefficients, C_λ^{mn} [14, 15], that can be refined by the procedure:

$$P_{hkl}(\alpha, \beta) = \sum_{\lambda=0}^{L} \sum_{m=1}^{M(\lambda)} \sum_{n=1}^{N(\lambda)} \frac{4\pi}{2\lambda+1} C_\lambda^{mn} K_\lambda^m(\Theta_{hkl}, \gamma_{hkl}) K_\lambda^n(\alpha, \beta), \quad (5)$$

where K_λ^m (Θ_{hkl}, γ_{hkl}) and K_λ^n (α, β) are the spherical harmonics; Θ_{hkl} and γ_{hkl} the angles between the [hkl] and [001] directions and between the [hk0] and [100] directions, respectively; $M(\lambda)$, $N(\lambda)$ depend on the crystal and sample symmetries, respectively, and on the maximum degree of the series expansion L (normally between 16 and 32) [14, 15].

Several spectra, collected at different α and β tilting angles, are to be fitted in order to refine correctly the texture coefficients. In this way the correlation between the roughness effect and the Debye–Waller factor can be worked out because the roughness contribution depends on θ and on the tilting angle α, whereas the Debye–Waller factors [12] rely on the diffraction angle θ only.

For the dependence of the profile shape on the angular position θ, an approach formerly developed is used [16], which allows us to express the HWHM and the Gaussianity content of a Pseudo-Voigt profile as a function of a mean crystallite dimension, D_{eff} and a microstrain parameter. Microstrain is defined as the standard deviation of the interplanar spacing from its mean value and can be related to the presence of dislocations or composition fluctuations. The effects of the antiphase domains, deformation and twin faults have been introduced following the theory by Warren [12], Patterson [17], Wagner [18] and Yuming *et al.* [19] for an f.c.c. crystal.

Antiphase domains contribute to broaden the superstructure reflections. When h, k, l indices are considered, with h and k having the same parity, e.g. $h + k$ = even, $k + l$ = odd, $l + h$ = odd, the component of the integral breadth due to the antiphase domain effects is:

$$\beta(2\theta) = \frac{\lambda\gamma(|h| + |k|)}{a\cos\theta\sqrt{h^2 + k^2 + l^2}}, \quad (6)$$

where λ is the radiation wavelength and γ is the probability of crossing a domain boundary within a distance equal to the cell parameter a.

Deformation and twin faults induce a shift, broadening and asymmetry in the profile. If α' and α'' are the intrinsic and extrinsic probabilities of deformation faulting, respectively, and β' the probability of twin faulting, the peak shift can be written as:

$$\Delta(2\theta)^\circ = \frac{90\sqrt{3}(\alpha' - \alpha'')\tan\theta}{\pi^2 h_0^2 (u+b)} \sum_b (\pm L_0), \quad (7)$$

using the symbols fully specified in Appendix B.

To account for the overall broadening we define an effective size D_{eff}, computed from the crystallite dimension D and from the deformation and twin fault probabilities in the following way [12]:

$$\frac{1}{D_{\text{eff}}} = \frac{1}{D} + \frac{[1.5(\alpha' + \alpha'') + \beta']}{a h_0 (u+b)} \sum_b |L_0|. \quad (8)$$

Peak asymmetry is evaluated from the extrinsic deformation and twin faulting probabilities. By defining y_1 as the intensity of the peak at the diffraction angle $2\theta_0 + x_2$, where $2\theta_0$ is the center of a fully symmetric profile, the peak asymmetry can be expressed as:

$$y_2 - y_1 = \frac{2A(4.5\alpha'' + \beta')}{c_2 x_2 \sqrt{3}\pi(u+b)} \sum_b (\pm) \frac{L_0}{|L_0|},$$

$$c_2 = 1 + \left\{ \frac{\lambda}{4\pi D_{\text{eff}} [\sin(\theta_0 + x_2) - \sin\theta_0]} \right\}^2. \quad (9)$$

Here, A is the area of the peak.

In conclusion the microstructure parameters to be refined by the present method are: the r.m.s. microstrain $\langle \epsilon^2 \rangle^{1/2}$ [16], the crystallite dimension D, the antiphasing probability γ, the two deformation faulting probabilities, α' and α'', and, finally, the twin faulting parameter, β'.

3. EXPERIMENTAL DETAILS

A commercial Ni_3Al intermetallic powder (Ni–23.3 Al–0.1 B at.%), initially ordered, was used in the experiments. The powder, having an initial grain diameter in the range of 50–200 μm, was milled using a vibratory ball-mill. The vials were sealed under an inert Ar atmosphere, after degassing the powder down to 10^{-2} torr, to prevent oxidation.

Different milling times were selected to follow the evolution of the disordering process: 3, 6, 17.5, 24 and 48 h. Each sample was observed with a Scanning Electron Microscope (SEM) to characterize its grain morphology after ball-milling, X-ray diffraction samples were prepared by back-side loading the powders into the sample holder and measured, as a first step, by a conventional Bragg–Brentano diffractometer. Such a preliminary analysis revealed preferred orientations to be present in the samples milled for intermediate times. Therefore all the milled samples were analysed by a Huber stress–texture goniometer using the experimental procedure fully described in [7].

Figure 1 shows a sketch of the geometrical arrangement of the apparatus. Several θ–2θ spectra in the 22–102° range were collected with a step of

0.04° and a 20 s counting time per step at different polar tilting angles α. The experimental tilting angles were selected on the basis of the actual texture of the specimens, which resulted to be fiberlike. The α angle was changed from 5° to 70° with a step of 5°. In this way 15 spectra were acquired for each sample.

4. RESULTS AND DISCUSSION

The fitting procedure described in the previous paragraph has been tested to analyse the XRD data obtained with heavily deformed Ni_3Al powders. Ball-milling is very effective in achieving high deformation levels in metallic specimens. Even though comparatively brittle, Ni_3Al can be highly deformed by ball-milling. The series of SEM micrographs in Fig. 2 shows how the original spherical shape [Fig. 2(a)] of the powder particles changes to platelike, after 7 h [Fig. 2(b)]. Further deformation leads to grain delamination [Fig. 2(c), sample milled for 17.5 h] suggesting fatigue to be one of the most active phenomena in the leading situation present in the milling experiments [20]. For the longest time the powder is reduced to micrometer size [Fig. 2(d)].

Figure 3 shows the evolution of the XRD patterns of the series of samples milled for increasing times. Mechanical grinding results in a progressive broadening of the diffraction peaks, as compared to the initial situation (unmilled sample). With respect to the starting pattern, the samples milled for longer times do also show the progressive weakening of

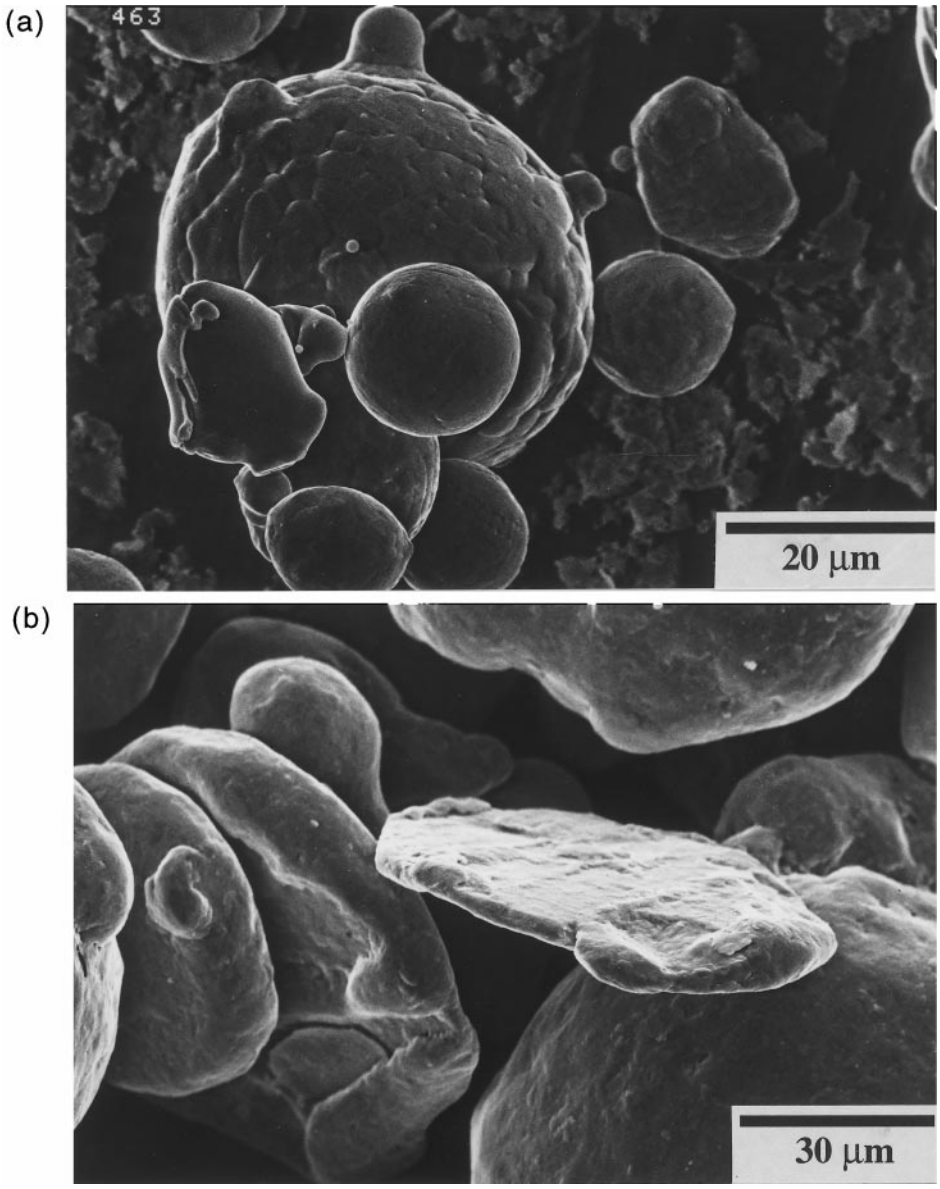

Fig. 2(a,b).

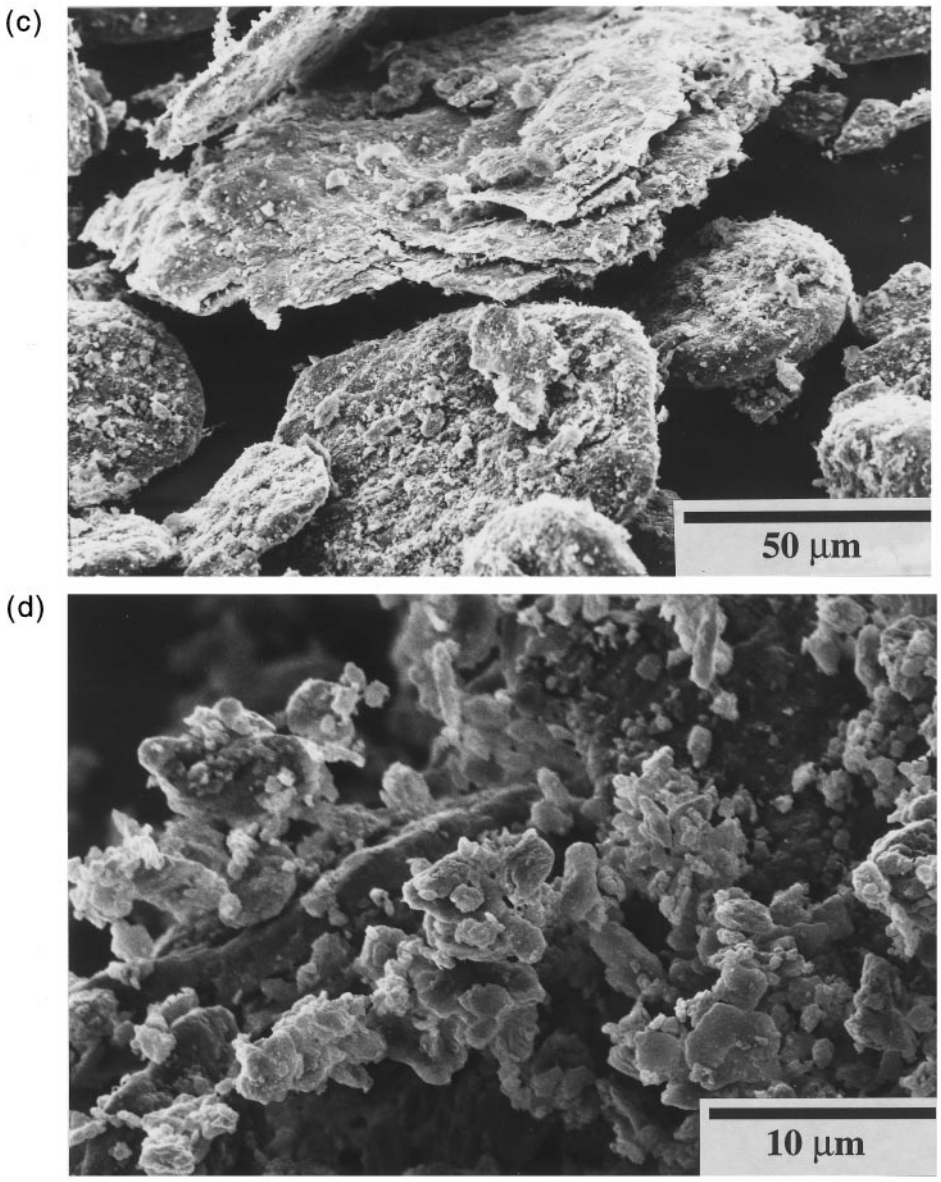

Fig. 2. SEM micrographs for the intermetallic powder, milled at increasing times, showing the evolution from spherical grains (a), to platelets (b), delaminated platelets (c) and to the final fine microstructure (d).

the superlattice peaks (marked *S* in Fig. 3), that are no longer detectable after about 24 h of milling. This corresponds to the progressive destruction of the long-range order inside the alloy. Deformation induced disordering is a well known phenomenon, observed in a number of intermetallics [21] and not last in Ni_3Al [22]. Through the characterization of the defects introduced by mechanical deformations it is possible to understand the way in which a disordered structure is achieved. We report in Fig. 4 the fitting results for the powder ball-milled for 17.5 h. The patterns, which were acquired at different α angles, show how the peak intensity changes as an effect of texture. Its effects on the diffracted intensity are evident in samples milled for times longer than 7 h. At this stage, as shown by Fig. 2(b), the particles have a platelike morphology.

Significant deviations of the powder pattern from the measured intensity are shown if texture is not taken into account in the refinement process. Figure 5 reports the results of the texture analysis for the sample milled for 17.5 h. Similar results were obtained for powders milled for longer times. The pole figures (111) and (220) were reconstructed from the texture coefficients C_λ^{mn} fitted by the program. They represent the intensity of the (*hkl*) reflection as a function of the polar and azimuthal angles of tilting (α and β, respectively, see Fig. 1).

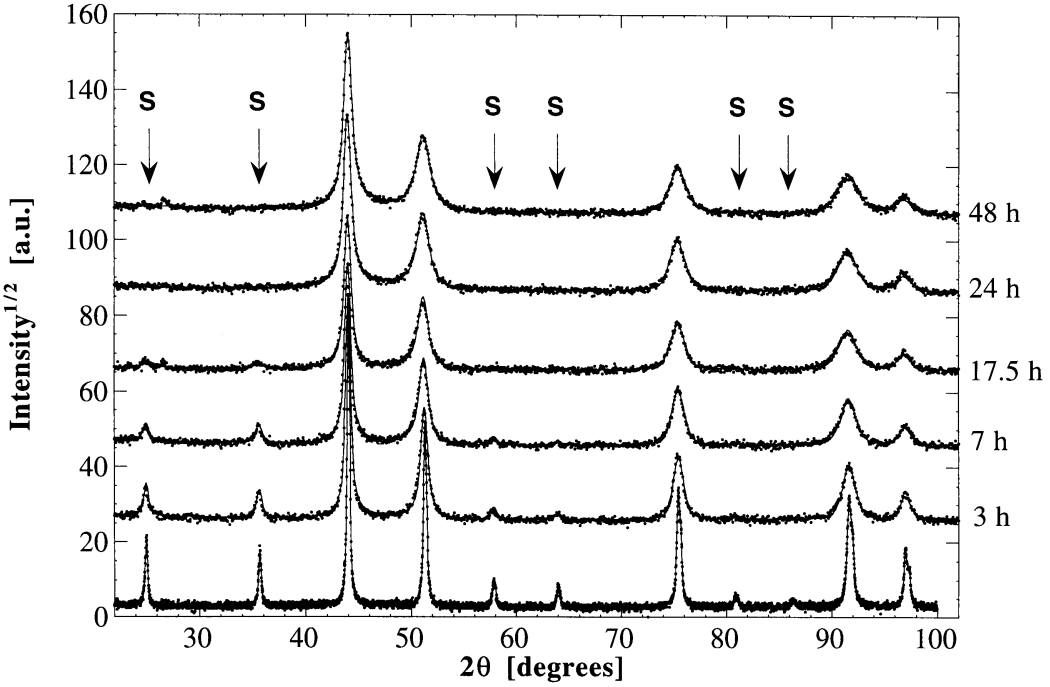

Fig. 3. Trend of the diffraction spectra at $\alpha = 0°$ for the samples milled for increasing time; the label S identifies the superstructure reflexes; dots represent the experimental points, lines the fitting functions.

As assumed in the refinement of the spectra, there is no variation of the pattern with the azimuthal angle. One way to look at this pole figure is by thinking that the intensity at the α, β is proportional to the number of crystallites oriented along the normal plane to the [*hkl*] direction, which is parallel to the direction identified by these angles. The normalized intensity assumes a value equal to 1 for a randomly oriented sample.

From Fig. 5 we can recognize that the 17.5 h sample shows a near (110) or (220) preferred orientation. Assuming that the platelike grains pile up in the sample holder along their base planes, we can conclude that the main axes of the grain are parallel

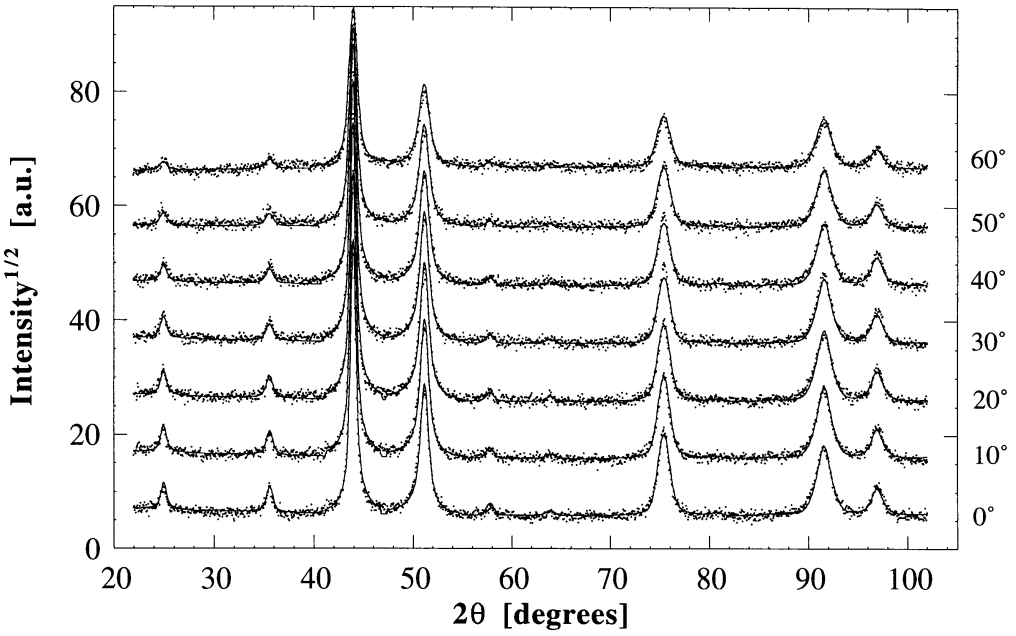

Fig. 4. Eight of the 15 spectra at different α angles, for the powder ball-milled for 17.5 h, collected to measure the texture of the sample; the fitting is represented by lines.

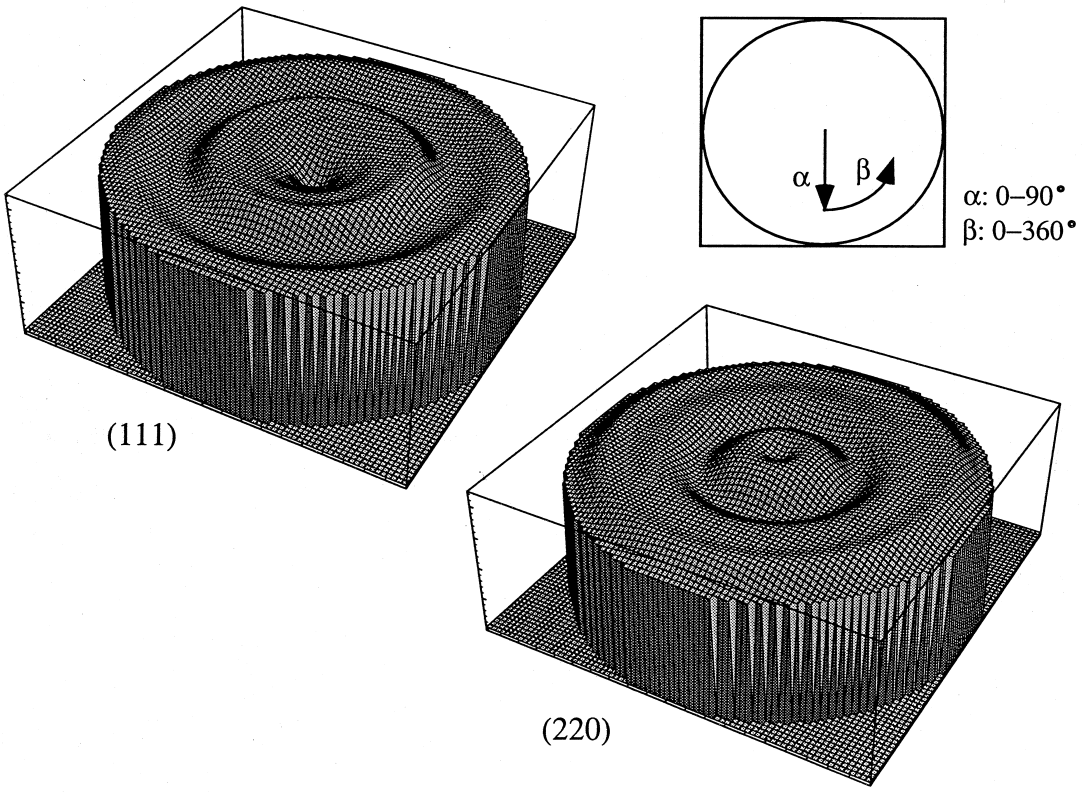

Fig. 5. Reconstructed pole figures (111) and (220) for the powder milled for 17.5 h to show the measured texture of the sample.

to the (110) plane (Fig. 6). This would be in agreement with the fact that a near (110) preferred orientation after rolling is typical for f.c.c. crystals [23]. When milling has reduced the grains to less than one micron [Fig. 2(d)] the texture is barely detectable as the powder is randomly arranged in the sample holder.

The accuracy of the method in evaluating the peak intensities was successfully tested in separating the surface roughness effect from the thermal vibration contribution. The first one is dependent on 2θ and α angles; whereas the second one is a function of θ only. The Debye–Waller (or thermal) factors were all found in the 0.35–0.65 Å^2 range, notwithstanding the significant roughness of the samples.

In the series of Fig. 7 we have summarized the results of the microstructural analyses of the intermetallic powders. The LRO parameter is plotted as a function of the milling time in Fig. 7(a). Starting from a value slightly lower than one, owing to the imperfect stoichiometry of the raw material, the LRO parameter goes down to zero, a value corresponding to a completely disordered alloy with a A_3B composition. In the same Fig. 6(a) it is possible to note that the probabilities of planar defects increase with milling time and reach a maximum value in the fully disordered sample. As to the probability of antiphase boundaries, the reported values refer to those samples with sufficiently strong superlattice reflections.

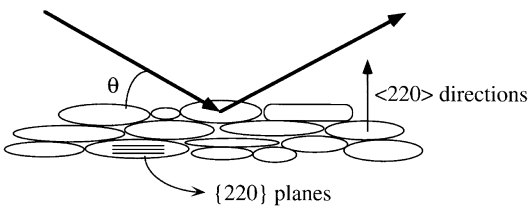

Fig. 6. Sketch of the pile-up of platelike grains in the sample holder.

Also the effect of twin faulting is difficult to account for in the case of those samples which were milled for the longest times, owing to the exceedingly high peak broadening.

Figure 7(b) represents the evolution of the r.m.s. strain and the average domain size D_{eff}. The major changes for these two parameters occur during the early stages of milling, when the degree of order in the alloy remains still comparatively elevated. The disordering kinetics appear to be faster than grain refinement and increase of the dislocation density, that, in this respect, can be considered to be disordering processes not so efficient as it seems to be the formation of planar faulting, i.e. intrinsic and extrinsic stacking faults.

A lattice expansion is also observed [Fig. 7(c)]. A less efficient atomic packing typical of the disor-

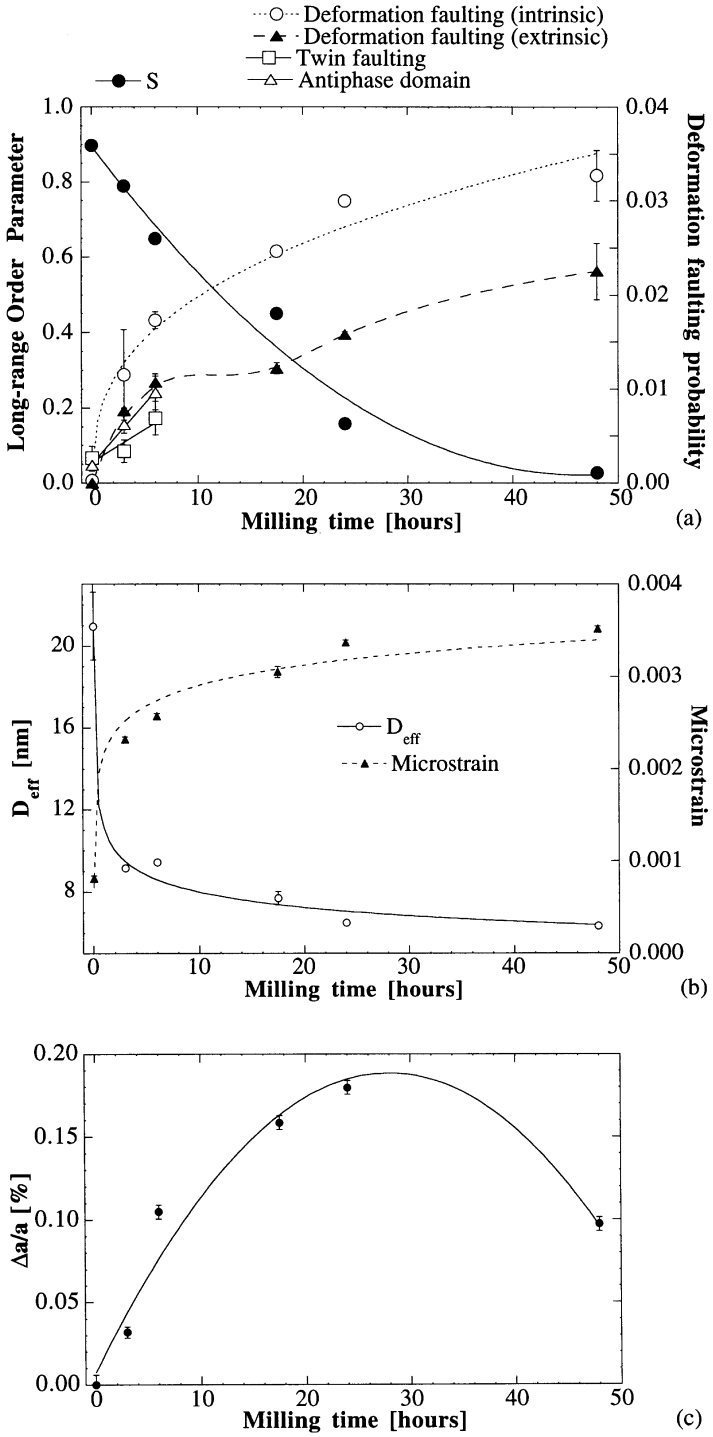

Fig. 7. Evolution of the microstructure with the milling time: (a) Long-Range Order parameter and planar defects, (b) crystallite size and r.m.s. microstrain, (c) lattice parameter as a deviation percentage from the cell constant of the unmilled sample.

dered state can be certainly invoked to justify this swelling, though the actual dependence of the lattice parameter on the degree of long-range order is also determined by the kind of point defects which are most likely to form [24]. For longer milling times this expansion is partially recovered, similarly to what we observed in other experiments [25]. When very high concentrations of point defects, such as vacancies and anti-sites, are reached, crystal structure crumbles down. This phenomenon may be enhanced by the surface energy associated with crystallite boundaries [26] and the increase in sur-

face energy due to dislocation cell boundaries [22]. If a surface energy of 1.4 J/m^2, an elastic modulus of 220 GPa and a Poisson ratio of 0.27 are assumed for Ni_3Al, it turns out that a strain difference of −0.00025 is obtained when crystallite size is reduced from 8 to 6 nm (see Fig. 7).

5. SUMMARY

We have presented a methodology to analyse powder diffraction spectra and applied it to the characterization of heavily deformed Ni_3Al powders. The method was successfully applied to these specimens and permitted us to follow the evolution of the microstructure and crystal structure during milling.

The deformation process was able to efficiently disorder the ordered starting powder down to the lowest degree of long-range order parameter compatible with this alloy composition. The progress of disordering is accompanied by the increase of twin faults and dislocations. The cell parameter increases as a result of the less efficient packing.

Ball-milling modifies also the shape of the powder grains from spheres into platelets with the two principal axes nearly parallel to the (110) crystallographic plane as found by the methodology. This is in agreement with what is normally found in cold-rolled f.c.c. polycrystals.

Acknowledgements—We kindly thank the ECC for the financial support (contract # CHRX-CT93-0324), and M. Baldessari and S. Setti for their help with XRD measurements. We would like to mention also J.R. Knibloe and R.N. Wright, Idaho National Engineering Laboratories for the supply of the Ni_3Al powder.

REFERENCES

1. Klug, H. P. and Alexander, L. E., *X-ray diffraction procedures for polycrystalline and amorphous materials*, 2nd ed. J. Wiley & Sons, New York, 1974.
2. Rietveld, H. M., *J. Appl. Cryst*., 1969, **2**, 65.
3. Lutterotti, L., Scardi, P. and Maistrelli, P., *J. Appl. Cryst*, 1992, **25**, 459.
4. Young, R. A. and Wiles, D. B., *J. Appl. Cryst*., 1982, **15**, 430.
5. Hill, R. J. and Madsen, I. C., *Powder Diffraction*, 1987, **2**, 146.
6. Hill, R. J. and Howard, C. J., *J. Appl. Cryst*., 1988, **21**, 86.
7. Ferrari, M. and Lutterotti, L., *J. Appl. Phys*., 1994, **76**, 7246.
8. Lutterotti, L., Polonioli, P., Orsini, P. G. and Ferrari, M., in *ASME Materials and Design Technology 1994* (Edited by T. J. Kozik). ASME, New York, 1994, Vol. 62, p. 15.
9. Wenk, H.-R., Matthies, S. and Lutterotti, L., *Mater. Sci. Forum*, 1994, **157–162**, 473.
10. Matthies, S., Lutterotti, L. and Wenk, H.-R., *J. Appl. Cryst*., 1997, **30**, 31.
11. Lutterotti, L., Matthies, S., Wenk, H.-R., Schultz, A. J. and Richardson, J., *J. Appl. Phys*. 1997, **81,** 594.
12. Warren, B. E., *X-ray Diffraction*, Addison-Wesley, Reading MA, 1969.
13. Hermann, H. and Ermrich, M., *Acta Cryst*., 1987, **A43**, 401.
14. Bunge, H. J., *Texture Analysis in Material Science*, Butterworths, London, 1982.
15. Roe, R.-J., *J. Appl. Phys*., 1965, **36**, 2024.
16. Lutterotti, L. and Scardi, P., *J. Appl. Cryst*., 1990, **23**, 246.
17. Patterson, M. S., *J. Appl. Phys*, 1952, **23**, 805.
18. Wagner, C. N. J., *Acta Metall*., 1957, **5**, 427.
19. Yuming, W. and Ziqung, Z., *Appl. Phys*., 1984, **A35**, 109.
20. Gialanella, S., Delorenzo, R., Marino, F. and Guella, M., *Intermetallics*, 1995, **3**, 1.
21. Koch, C. C., in *Materials Science and Technology* (Edited by R. W. Cahn, P. Haasen and E. J. Kramer). Weinheim VCH, 1991, Vol. 15, 193.
22. Jang, J. S. C. and Koch, C. C., *J. Mater. Research*, 1990, **5**, 498.
23. Barrett, C. and Massalski, T. B., in *Structure of Metals* (Edited by 3rd), Pergamon Press, Oxford, 1980.
24. Bakker, H., Zhou, G. F. and Yang, H., *Mater. Sci. Forum*, 1995, **47**, 179–181.
25. Gialanella, S., Lutterotti, L., Barò, L., Surinach, S., Le Caër, G. and Delcroix, P., submitted to *Acta Material.*
26. Lutterotti, L., Di, Maggio R. and Cappuccio, G., submitted to *J. Amer. Ceram. Soc.*

APPENDIX A

Composition–occupancy definitions and relations

The following definitions can be found also in the book of Warren [12]; they are reported here only for more readability of the paper.

For a binary alloy composition A_xB_y and a crystal structure with two different sites α and β, these quantities can be defined:

r_α = fraction of α-sites occupied by the atom A,
w_α = fraction of α-sites occupied by the atom B,
r_β = fraction of β-sites occupied by the atom B,
w_β = fraction of β-sites occupied by the atom A,
x_A = fraction of atom A in the composition,
x_B = fraction of atom B in the composition,
y_α = fraction of α-sites,
y_β = fraction of β-sites.

As a consequence, the following relations are obvious:

$$r_\alpha + w_\alpha = 1, r_\beta + w_\beta = 1, y_\alpha + y_\beta = 1, \quad x_A + y_B = 1. \tag{A1}$$

$$r_\alpha y_\alpha + w_\beta y_\beta = x_A, r_\beta y_\beta + w_\alpha y_\alpha = x_B. \tag{A2}$$

APPENDIX B

Additional definitions for equations (6)–(8)

For an f.c.c. crystal, additional definitions are needed to compute equations (6) to (8):

$$L_0 = h + k + l, \tag{B1}$$

$$h_0^2 = h^2 + k^2 + l^2. \tag{B2}$$

Each diffraction peak in a powder pattern can be composed by different (*hkl*) components. Some components, for which $L_0 = 3n \pm 1$ (n is an arbitrary integer), are broadened by faultings and the others are said to be unbroadened. Following this definition u is the number of

unbroadened components and b the number of broadened ones. Therefore the summations in the equations (6)–(8) are performed only on the broadened components (this is the meaning of the subscript b) and the symbol ($\pm$) indicates that the sign (+) must be used if $L_0 = 3n + 1$ and the (−) sign for $L_0 = 3n - 1$.